Deformation-induced long-range internal stresses and lattice plane misorientations and the role of geometrically necessary dislocations

H Mughrabi

Deformation-induced long-range internal stresses and lattice plane misorientations and the role of geometrically necessary dislocations

Journal:	*Philosophical Magazine & Philosophical Magazine Letters*
Manuscript ID:	TPHM-05-Oct-0465.R1
Journal Selection:	Philosophical Magazine
Date Submitted by the Author:	30-Nov-2005
Complete List of Authors:	Mughrabi, H; Universität Erlangen-Nurnberg, Inst Werkstoffwissenschaften, Lehrstuhl 1
Keywords:	X-ray topography, deformation mechanisms, transmission electron microscopy, X-ray diffraction
Keywords (user supplied):	internal stresses, geometrically necessary dislocations

Deformation-induced long-range internal stresses and lattice plane misorientations and the role of geometrically necessary dislocations

HAEL MUGHRABI

Institut für Werkstoffwissenschaften, Allgemeine Werkstoffeigenschaften,

Universität Erlangen-Nürnberg, Martensstr. 5, D-91058 Erlangen, Germany

Abstract

The goal of this study is to develop a unified picture of the role of geometrically necessary dislocations (GNDs) in the evolution of long-range internal stresses and lattice plane misorientations in the heterogeneous dislocation pattern of deformed crystals. For this purpose, X-ray diffraction techniques are considered as the pertinent experimental tools. On the modelling side, the composite models of single/multiple slip serve to interpret the experimentally measured long-range internal stresses quantitatively in terms of densities of GNDs. However, in order to be able to deduce from experiment the evolution of those GNDs that are responsible for the observed lattice plane misorientations, the composite model must be refined. Quite generally, one and the same GND array can give rise to both long-range internal stresses and lattice plane misorientations.

On this basis, available experimental data obtained on cyclically and tensile-deformed copper (and copper-manganese) single crystals were analyzed quantitatively. The stresses acting locally in the "hard" dislocation cell walls and in the "soft" cell interiors and the magnitude of the internal stresses are found to increase approximately linearly with the applied stress. In spite of the fact that the density of the GNDs always amounts to only a few per cent of the total dislocation density, they are responsible for the long-range internal stresses and/or for the misorientations. An analysis of the evolution of the lattice plane misorientations shows that the kink walls and the dislocation sheets/grids in stage II are geometrically necessary boundaries (GNBs), whereas the dislocation cell walls formed by multiple slip are incidental dislocation boundaries (IDBs).

Keywords: deformation mechanisms, geometrically necessary dislocations, internal stresses, misorientations, X-ray topography, transmission electron microscopy

---

Email: mughrabi@ww.uni-erlangen.de

1. Introduction

During plastic deformation of crystalline materials, dislocations multiply and assemble in heterogeneous dislocation distributions such as dislocation tangles, bundles, wall and cell structures, compare the reviews by Frank Nabarro (to whom this article is dedicated), Holt and Basinski [1] and by others [2,3,4,5]. In addition to the increasing dislocation density, the evolution of deformation-induced long-range internal stresses [5,6,7] and increasing lattice plane misorientations [8,9,10] are important features of the evolving dislocation pattern. These features are manifestations of the evolution of a non-homogeneous deformation on a microscale, in spite of the fact that, on a macroscopic scale, deformation is homogeneous. A characteristic of this non-homogeneous deformation is the accumulation of local *"excess dislocations"* of one sign.

Today, it has become common practice to refer to these excess dislocations as *"geometrically necessary"* dislocations (GNDs), almost irrespective of whether they are necessary or not. In the original introduction of GNDs by Cottrell [11] and later by Ashby [12], the definitions differed somewhat. In the present paper, we shall retain the term GNDs, but only after making some hopefully clarifying remarks. Cottrell, referring to "more macroscopic aspects of dislocation geometry", clearly had macroscopic non-homogeneous deformation modes such as bending or twisting in mind when stating that "dislocations (i.e. GNDs) are necessary to accommodate the non-uniform strains". Ashby related the GND density to gradients of deformation occurring in "plastically non-homogeneous" materials and considered in particular particle-hardened materials. Thus, he referred to GNDs on a microstructural scale. Frank Nabarro questions the justification of the term "geometrically necessary" and sees it as a chicken and egg problem [13]. He asks: "Does the geometry (sharp interfaces or lattice curvatures) make the dislocations necessary or do "excess dislocations" cause the geometry?" The difficulty to define precisely what is meant is reflected in the diversity of the different contributions to the Scripta Materialia Viewpoint Set on "Geometrically Necessary Dislocations and Size-Dependent Plasticity" [14]. A number of the contributors emphasized the importance of the *scale* in considerations of GNDs.

In the following, we find the formulation in the Introduction to this Viewpoint Set by Needleman and Gil Sevillano [15] helpful: "…..For the bent beam, the gradient of deformation is associated with the macroscopically imposed strain field. But even if the imposed field is macroscopically uniform, as in simple tension, dislocation structures develop

that lead to locally non-uniform deformation fields. *These dislocation structures, which are also referred to as GNDs although the geometric necessity is lacking ,* can give rise to…." . This latter formulation corresponds to the author's views, as expressed above and repeatedly before. The present work is dealing with macroscopically homogeneous and microscopically nonhomogeneous uniaxial tensile and cyclic deformations, in which GNDs are induced by and stored in the heterogeneous dislocation pattern.

In the present context, it is stressed that these GNDs can give rise to both deformation-induced long-range internal stresses and/or lattice plane misorientations. The limited available experimental data which allow to substantiate this statement have been obtained mainly in classical standard X-ray diffraction experiments. The advantage of X-ray diffraction lies in the fact that, with this one technique, quantitative information on the dislocation density and the lattice plane misorientations and a measure for the arrangement of dislocations can be obtained on a larger scale of some 100 μm [9]. A prime goal of this study will be to reassess existing data in an attempt to develop a unified picture. The available data will be evaluated with the aim to derive semi-empirical laws of evolution of both long-range internal stresses and lattice plane misorientations as a function of deformation. The long-range internal stresses will be discussed in the framework of the author's composite model for single and multiple slip [16,6,7]. The lattice plane misorientations observed after tensile deformation in single slip will be assessed in terms of a recently developed microstructure-based model of the broadening of X-ray rocking curves [10], and a new evaluation of deformation-induced misorientations and long-range internal stresses evolving in multiple slip will be presented.

2. Long-range internal stresses, the density of GNDs and the flow stress

2.1 Single slip

The formulation of the composite model for single slip was first developed in order to deal with the (localized) cyclic shear plasticity in the wall structure of persistent slip bands (PSBs) in fatigued metals [16,6,7]. The existence of deformation-induced long-range internal stresses (forward stresses in the "hard" walls and back stresses in the "soft" channels between the walls) was evidenced by transmission electron microscopy (TEM) [6] and by X-ray diffraction [7] and has been discussed in detail earlier. Here, we are mainly interested in the GNDs which build up at the interfaces between the walls and the channels, as illustrated in figure 1, and act as sources of internal stresses, leading to a redistribution of the local stresses and thereby ensuring compatible plastic deformation. Before proceeding to a more

quantitative treatment, it is noted in passing that, in figure 1, it is assumed that the PSB lamella is embedded in the surrounding matrix structure in such a fully constrained manner that any lattice plane bending accompanied by tilt misorientation due to the GNDs is suppressed.

Now, if the *local* shear flow stresses of PSB channels and walls are τ_c and τ_w, respectively, then these local flow stresses are identical to the sums of the macroscopic shear flow stress τ and the corresponding deformation-induced long-range internal stresses, the back stress $\Delta\tau_c$ in the channels and the forward stress $\Delta\tau_w$ in the walls, respectively:

$$\tau_c = \tau + \Delta\tau_c \quad (1)$$

and

$$\tau_w = \tau + \Delta\tau_w \, . \quad (2)$$

The deformation-induced long-range internal stresses can be expressed in terms of the corresponding plastic and elastic shear strains $\gamma_{pl,c}, \gamma_{pl,w}$ and $\gamma_{el,c}, \gamma_{el,w}$, respectively, as:

$$\Delta\tau_c = -G\Gamma f_w(\gamma_{pl,c} - \gamma_{pl,w}) = +G\Gamma f_w(\gamma_{el,c} - \gamma_{el,w}) \quad (3)$$

and

$$\Delta\tau_w = +G\Gamma f_c\,(\gamma_{pl,c} - \gamma_{pl,w}) = -G\Gamma f_c\,(\gamma_{el,c} - \gamma_{el,w}), \quad (4)$$

where f_c and f_w are the volume fractions of channels and walls, respectively, G is the shear modulus and Γ is Eshelby's elastic accommodation factor ($\Gamma \leq 1$) which has been introduced in a rather formal sense and which will be commented upon later in more realistic terms, compare Section 4. It should be noted that the internal stresses can be written alternatively in terms of the plastic strain mismatch ($\gamma_{pl,c} - \gamma_{pl,w}$) or the equivalent negative elastic strain mismatch, i.e. $-(\gamma_{el,c} - \gamma_{el,w})$. The latter can then be converted easily into corresponding shear flow stresses via Hooke's law.

We turn now to the GND density in more detail than in earlier work [6,7], There, it was shown that the line density of the GNDs, n, measured along the normal to the glide plane, is:

$$nb = (\gamma_{el,w} - \gamma_{el,c}) = \frac{\tau_w - \tau_c}{G}, \quad (5)$$

where b is the modulus of the Burgers vector. By averaging the local density of the GNDs over the wall spacing d, the mean GND density is obtained as

$$\rho_{GND} = \frac{2n}{d} = \frac{2(\tau_w - \tau_c)}{bGd} \, . \quad (6)$$

Thus, the spatially averaged GND density is directly proportional to the difference between the local flow stresses in the hard and soft regions and inversely proportional to the wall

spacing. Via equations 3 and 4 and making use of equation 5, ρ_{GND} can also be formulated in terms of the internal stresses as

$$\rho_{GND} = \frac{2\Delta\tau_w}{bdGIf_c} = \frac{-2\Delta\tau_c}{bdGIf_w}, \quad (7)$$

or, inserting equations 1 and 2 in equation 6, in terms of the difference $\Delta\tau_w$ - $\Delta\tau_c$ as

$$\rho_{GND} = \frac{2(\Delta\tau_w - \Delta\tau_c)}{bdGI} . \quad (8)$$

Finally, it is recalled that, in the composite model, the macroscopic flow stress τ is expressed in terms of the rule of mixtures as

$$\tau = f_c\tau_c + f_w\,\tau_w . \quad (9)$$

This set of relations provides a complete basis for a thorough analysis., as will be shown below for the PSB wall structure.

2.1.1 Example of persistent slip bands (PSBs) in fatigued fcc metals

All quantities introduced above can be obtained from experiment, as was shown first in the analysis of the PSB wall structure in fatigued copper single crystals [6,7]. In this case, the cyclic flow stress of PSBs at room temperature is $\tau_{PSB} \approx 28$ MPa. According to the most recent estimate [17], τ_c results from the partial superposition of a dipolar passing stress and an Orowan bowing stress of the bowed-out screw dislocations in the channels and is found to be $\tau_c \approx 17.7$ MPa. Taking the mean values of the local stresses τ_w that were determined by measurement of the radii of curvature of bowed-out edge dislocations at the periphery of the dislocation walls, one obtains $\tau_w \approx 65$ MPa [6]. Thus, the approximate relationships

$$\tau_c \approx 0.63\ \tau_{PSB},\ \Delta\tau_c \approx -0.37\ \tau_{PSB} \quad (10)$$

$$\text{and } \tau_w \approx 2.3\ \tau_{PSB}\ ,\ \Delta\tau_w \approx +1.3\ \tau_{PSB} \quad (11)$$

follow. In the case of copper, the only data available are those discussed here which refer to cyclic deformation at room temperature. Hence, the evolution of the GND density ρ_{GND} and the internal stresses $\Delta\tau_c$ in the channels and $\Delta\tau_w$ in the walls as a function of different macroscopic shear flow stresses τ_{PSB} cannot be determined. However, in the case of nickel single crystals, deformed cyclically at four different temperatures between 77 and 750 K, Hieckmann [18] has produced complete sets of data of internal stresses by analysis of asymmetrically broadened X-ray diffraction profiles, compare [19]. From Hieckmann's data, the following approximate relationships follow: $\tau_c \approx 0.77\ \tau_{PSB}$ and and $\tau_w \approx 2.0\ \tau_{PSB}$. These relationships, referring to four different temperatures and PSB stresses in the range from ca.

10 to ca. 100 MPa, compare favourably with the above results (relations 10 and 11) obtained on copper single crystals deformed cyclically at room temperature.

Next, the GND density ρ_{GND} of the GNDs in PSBs in copper can be estimated according to equation 6 (or, alternatively, equations 7 or 8). Using the values $\tau_c \approx 17.7$ MPa, $\tau_w \approx 65$ MPa, $G = 42000$ MPa, $d = 1.4$ µm [6,7], we obtain $\rho_{GND} \approx 6.7\times10^{12}$ m^{-2}. Since the mean dislocation density in the PSB wall structure is ca. 5×10^{14} m^{-2}, this implies that the GND density is quite low and represents only little more than 1% of the total dislocation density, as concluded earlier [6].

2.2 Multiple slip

Assuming an idealized dislocation cell structure, as indicated schematically in figure 2, the composite model has also been developed for symmetrical multiple slip. Essentially, a similar set of equations as before (equations 1 to 9) can be written down, as reported elsewhere [6,7,19]. Here, we shall confine ourselves to those features of the model that differ from the case of single slip and that are relevant to the role of GNDs as sources of internal stresses. Referring to figure 2, it is clear that, for ideally symmetric multiple slip, no lattice plane misorientations will be expected to develop. On the other hand, in the model shown in the figure, long-range internal stresses will arise as follows. Axial internal stresses are induced by pairs of dislocations of Burgers vectors $\mathbf{b}_1$ and $\mathbf{b}_2$ on two symmetric slip systems. These dislocation pairs can be considered as resultant dislocations with the Burgers vector $\mathbf{b}_{res}$ lying parallel to the stress axis. It is expedient to formulate all stresses alternatively as axial stresses σ or resolved shear stresses τ, depending on which is more appropriate, keeping in mind that $\tau = \phi\sigma$, where ϕ is the corresponding Schmid factor. Similarly, axial strains $\varepsilon \approx \phi\gamma$ (for small strains) can be formulated in terms of the resolved shear strains γ. In the case of [001]-orientated fcc crystals, $\phi = 0.408$.

Proceeding as before, the density (in terms of "resultant" dislocations of Burgers vector $\mathbf{b}_{res}$) of *those GNDs which are responsible for the internal stresses* follows as:

$$\rho_{GND} = \frac{2n}{d} = \frac{2(\sigma_w - \sigma_c)}{b_{res} E d} \quad . \tag{12}$$

Here, E is Young's modulus and d is the transverse cell wall spacing. This approach is only approximately correct, since it does not take into account Poisson contraction. Alternatively, in analogy to equation 7, ρ_{GND} can also be expressed in terms of the axial internal stresses $\Delta\sigma_w$ and $\Delta\sigma_c$ in the dislocation cell walls and cell interiors, respectively:

$$\rho_{GND} = \frac{2\Delta\sigma_w}{b_{res} d_c E f_c} = \frac{-2\Delta\sigma_c}{b_{res} d_c E f_w} . \quad (13)$$

In relation (13), the Eshelby factor Γ does not appear, because it has been argued that, in this case, $\Gamma \approx 1$ [19]. Finally, in analogy to equation 8, ρ_{GND} can also be written as:

$$\rho_{GND} = \frac{2(\Delta\sigma_w - \Delta\sigma_c)}{b_{res} dE} . \quad (14)$$

It is interesting to compare some numerical data for different deformations of tensile-deformed [001]-orientated copper single crystals which were studied in detail by X-ray diffraction [6,7,19]. Here, the results of the analysis of two states of deformation, i) and ii), characterized by the resolved shear stresses τ and shear strains γ., will be reported. In the analysis, the following values were used: $\Delta\tau_c$ and $\Delta\tau_w$ (from [19], corrected according to [20] and converted to $\Delta\sigma_c$ and $\Delta\sigma_w$), d obtained by TEM [19] and the total dislocation densities ρ from [19,21]. Finally, with the values ρ_{GND}, as estimated via equation 14 (with (E = 67000 MPa), the ratios ρ_{GND}/ρ could be determined. The complete sets of data obtained are:

i) τ = 26.2 MPa, γ = 0.068, τ_c = 23.3 MPa, $\Delta\tau_c$ = -2.9 MPa, τ_w = 38.4 MPa, $\Delta\tau_w$ = +12.2 MPa, d = 2.3 µm, $\rho_{GND} = 1.36\times10^{12}$ m^{-2}, $\rho = 6.8\times10^{13}$ m^{-2}, $\rho_{GND}/\rho \approx 0.020$.

ii) τ = 75.6 MPa, γ = 0.52, τ_c = 67.0 MPa, $\Delta\tau_c$ = -8.6 MPa, τ_w = 101.3 MPa, $\Delta\tau_w$ = +25.7 MPa, d = 0.8 µm, $\rho_{GND} = 8.79\times10^{12}$ m^{-2}, $\rho = 3.46\times10^{14}$ m^{-2}, $\rho_{GND}/\rho \approx 0.025$.

Before discussing these exemplary results, it is emphasized that the results for ρ_{GND} are only quantitatively correct within a numerical factor of ca. 2, because the simple dislocation glide geometry assumed in the model (figure 2) does not correspond accurately in detail to the crystallography of the slip systems of [001]-orientated single crystals. The following findings are considered noteworthy:

- The deformation-induced internal stresses increase with increasing deformation. A more detailed analysis [22] shows that the evolution of the local shear flow stresses and of the deformation-induced internal stresses can be represented by the following simple approximate relations:

$$\tau_c \approx 0.9\ \tau,\ \Delta\tau_c \approx -0.1\ \tau, \quad (15)$$

and

$$\tau_w \approx 1.4\ \tau,\ \Delta\tau_w \approx +0.4\ \tau . \quad (16)$$

- The density ρ_{GND} of the GNDs is small and of the same order of magnitude as discussed in Section 2.1.1 for the case of PSBs. Also, ρ_{GND} increases with increasing deformation and total dislocation density ρ. Nonetheless, the ratio ρ_{GND}/ρ seems to stay approximately constant within the accuracy of the evaluation. This conclusion

corresponds to a similar result deduced from a determination of ρ_{GND} by an analysis of the X-ray rocking curve broadening observed on copper single crystals that were deformed in tension in single slip into stage II of the work-hardening curve [10].

A more detailed analysis and discussion of these data will be presented elsewhere [22]. Here, it is noted that relations (15) and (16) seem to represent a quite general result. Thus, an analysis of X-ray data of Hilscher (reported in [20]) on tensile-deformed [001]-orientated single crystals of the substitutional alloy Cu-1.4at.%Mn also yields similar relationships. Figure 3 shows a plot of the local flow stresses $(\tau_w - \tau_o)$ and $(\tau_c - \tau_o)$ in the cell interiors and in the cell walls, respectively, corrected for the solid solution friction stress $\tau_o \approx 10$ MPa, against the applied flow stress $(\tau - \tau_o)$, also corrected for τ_o. The results, formulated in analogy to relations 15 and 16, can be expressed as $(\tau_c - \tau_o) \approx 0.87(\tau - \tau_o)$ and $(\tau_w - \tau_o) \approx 1.43(\tau_w - \tau_o)$, respectively, and are found to be almost identical to the results obtained above for deformed [001]-orientated copper crystals. Finally in support of the conclusion that these results are quite general, it is noted that Hieckmann [18] has also found similar relationships between the local stresses and the applied stress in the case of tensile-deformed nickel single crystals of not only multiple slip but also single slip orientations.

2.3 The effect of GNDs on the flow stress

According to Ashby [12], the simplest possible "dimensionally correct" expression for the flow stress of a material containing, in addition to a density ρ_S of statistically stored dislocations , also a density ρ_{GND} of GNDs is given by the following Taylor-type flow stress law:

$$\tau = \alpha G b \sqrt{\rho_S + \rho_{GND}}\,, \qquad (17)$$

Here, α is a geometrical constant (arrangement factor), and the densities ρ_S and ρ_{GND} are spatially averaged values. In the author's opinion, this expression needs refinement as follows. First, as shown in a more detailed consideration of the composite model [7,23,24], it can be concluded that only under conditions of multiple slip, when GNDs act as forest dislocations to glide dislocations do the GNDs make an appreciable contribution to the flow stress. Next, it must be taken into account that the dislocation density varies in space. With these arguments, it becomes clear that only a *local* space-dependent flow stress can be defined for a given site. In a simple one-dimensional picture, the variation of the local flow stress $\tau_{loc}(x)$ as a function of the coordinate x would then be given by

$$\tau_{\mathrm{loc}}(x) = \alpha G b \sqrt{\rho_{\mathrm{S}}(x) + \beta \rho_{\mathrm{GND}}(x)}\,, \tag{18}$$

where the constant β ($0 < \beta < 1$) takes into account globally that only a fraction of the GNDs contributes to a certain extent to the flow stress [7,23]. The macroscopic flow stress τ is then given by the spatial average of the local flow stresses, i.e.

$$\tau = \langle \tau_{\mathrm{loc}}(x) \rangle\ . \tag{19}$$

It should be noted that the rule of mixtures (equation 9) is only a special case of equation 19.

3. Lattice plane misorientations and the density of GNDs as a function of deformation

Lattice plane misorientations manifest themselves in TEM in spatially varying background "orientation contrast" that changes in a characteristic manner when the specimen is tilted. In principle, the axes of misorientation (twist and/or tilt) can be determined by inspecting different crystallographic sections under different angles of tilt. This technique is time- and specimen-consuming and can only yield qualitative results on a microstructural scale. On the other hand, the analysis of X-ray rocking curve broadening, measured on different crystallographic sections, taking into account also the variation for different so-called azimuthal angles [9,10], provides a global quantitative measure of the strength of the misorientations and allows also the determination of the dominant tilt and twist axes. As a complementary technique, X-ray Berg-Barrett topography with its much larger field of view than TEM can provide on a more global scale similar but somewhat less quantitative information. In addition, the dominant crystallographic directions are easily recognized in the topographs [8,10,25].

In face-centred cubic (fcc) single crystals deformed in single slip, dominant features of the dislocation arrangements are primary dipolar edge dislocation clusters in the form of braids and bundles, also as kink walls, and planar sheets or grids (which lie roughly parallel to the primary glide plane) in tensile deformation [1,2,3,4,5]. In cyclic deformation, the dipolar edge dislocations accumulate in so-called veins in the matrix and in dislocation walls in the PSBs, compare [26]. In both cases, the deformation-induced misorientations due to these dipolar edge patterns are mainly to-and-fro tilts around an axis along the line direction of the edge dislocations. Referring to the primary slip system $[\bar{1}01](111)$, the axis of tilt would be $[1\bar{2}1]$.

3.1 Lattice plane misorientations after cyclic deformation in single slip

In the case of cyclically deformed single crystals, only qualitative information is available. It has been shown by measurements of X-ray rocking curves that the misorientations observed are always much smaller than those found after tensile deformation [27]. This is probably a result of the much smaller dislocation glide paths in cyclic, compared to unidirectional deformation. TEM and X-ray Berg-Barrett topography reveal only negligible orientation contrast across individual dipolar dislocation veins and walls. However, in the case of the PSB dislocation walls and the walls found at higher amplitudes, both techniques show that there are also more appreciable misorientations with a much larger wavelength extending over some ten dislocation walls [28], compare the low-magnification TEM micrograph and the Berg-Barrett topograph of the primary glide plane shown in figure 4. These observations document that kink-wall-like dislocation structures exist which are separated by some ten walls. These kink walls are probably related to the surface patterns observed in cyclically deformed copper single crystals long ago [29]. As a complementary information, figure 5 shows a low-magnification TEM micrograph of the $(1\bar{2}1)$-section of a copper single crystal that had been cyclically deformed at a higher plastic strain amplitude. Again, misorientations are recognized between regions separated by a larger number of dislocation walls. The details of the misorientations revealed depend on the diffraction conditions [28]. Crudely speaking, it is found that, in addition to the $[1\bar{2}1]$-axis of tilt, also a [111]-axis of twist is responsible for the misorientations observed. Similar more large-scale features of the dislocation patterns are also apparent in more recent ECC/SEM studies (ECC: electron channelling contrast, SEM: scanning electron microscopy) on individual grains of cyclically deformed nickel polycrystals [30] and on cyclically deformed copper single crystals [31].

In view of the rather short dislocation glide paths in cyclic deformation, it is at present unclear how such subtle details with rather long-range periodicities develop in the dislocation patterns. It appears likely that the rather small broadening of the rocking curves of cyclically deformed copper single crystals [27] is caused mainly by these kink-wall-like structures and that most of the GNDs responsible for the misorientations are located in them, i.e. in only a fraction of the walls which are separated by larger distances. At the same time, however, there must be additional GNDs located on either side of each wall (with densities ρ_{GND} as given by

equations 5 to 8) so as to provide the internal stresses that are required to allow simultaneous deformation of the channels and walls.

3.2 Lattice plane misorientations after tensile deformation in single slip

The information on deformation-induced lattice plane misorientations found after tensile deformation of fcc crystals is much more detailed than that discussed above for cyclic deformation, compare some of the early work [32,33] and the more detailed later studies [8,9,10,25,28]. As discussed in some detail in [10], a difficulty existed in the unambiguous evaluation of the broadened X-ray rocking-curve half-width $\Delta\beta_{1/2}$ (which is proportional to the mean angle of misorientation β) in terms of microstructural parameters. Recently, the author introduced microstructural models for the dominant dislocation patterns introduced during stage II work hardening, namely for the kink walls which lie perpendicular to the primary Burgers vector $[\bar{1}01]/2$ and the so-called sheets/grids which are layer-like dislocation networks consisting of primary and secondary dislocations and their reaction products and which lie roughly parallel to the primary glide plane (111), compare [1,2,3,4,5]. In these models, the rocking-curve half-width $\Delta\beta_{1/2}$ is related to the density ρ_{GND} of GNDs and the flow stress (or strain) in terms of known parameters of deformation. The arrangement of the GNDs in the dislocation kink walls observed in stage II of deformed fcc single crystals, as shown in figure 6, was represented in an idealized model (figure 7) which resembles the earlier model by Mader and Seeger [34], and the following relationship [10] was derived:

$$\Delta\beta_{1/2} \approx \frac{3\theta_{II}\Lambda}{2\alpha^2 G^2 b} \cdot \frac{\rho_{GND}}{\rho} \cdot \tau \approx 0.0169 \frac{\rho_{GND}}{\rho} \cdot \tau \,. \qquad (20)$$

Here, θ_{II} is the stage II work hardening coefficient, and Λ is the proportionality constant in the relationship between the dislocation glide path and the shear strain in stage II. In figure 8, the rocking-curve halfwidths $\Delta\beta_{1/2}$ (maximum values for the appropriate azimuthal orientations), taken from a fair number of partly unpublished rocking-curves which had been measured on copper single crystals deformed into stage II at room temperature and at 77 K, see [10] for details, are shown in a plot of $\Delta\beta_{1/2}$ versus τ. Within the scatter of the data, $\Delta\beta_{1/2}$ increases linearly with the flow stress τ. This finding has the following implications:

- Since the flow stress τ and the shear strain γ are linearly related in stage II, the rocking curve half-width is also directly proportional to the shear strain γ, i. e. $\Delta\beta_{1/2} \propto \gamma$. In terms of Pantleon's model of lattice plane misorientations [35,36], this means that, in the terminology of Kuhlmann-Wilsdorf and Hansen [37], dislocation kink walls are

so-called *geometrically necessary boundaries*, GNBs, in contrast to *incidental dislocation boundaries*, IDBs.

- The ratio ρ_{GND}/ρ seems to be fairly constant in stage II. Of course, this statement applies strictly only to *those GNDs that are responsible for the tilt misorientations* and not necessarily to all GNDs, compare Section 4. From the slope of the straight line drawn through the data points in figure 8, the ratio ρ_{GND}/ρ is found to be about 0.047 via equation (20). This implies that the GNDs responsible for the tilt misorientations comprise only less than 5% of the total dislocation density. This result is considered to be entirely reasonable.

Based on less detailed available X-ray rocking curve data than in the preceding case, the twist misorientations of the sheets/grids around the normal to the glide plane were also evaluated in terms of a simple microstructural model [10] which is discussed in greater detail in ref. [22]. Again, a linear relationship was found between $\Delta\beta_{1/2}$ and τ, allowing the conclusion that the sheets/grids must also be considered as GNBs.

3.3 Lattice plane misorientations after tensile deformation in multiple slip

In the case of tensile-deformed [001]-orientated copper single crystals, there exist fortunately both detailed X-ray diffraction measurements of long-range internal stresses, as discussed in Section 2.2, and also X-ray rocking-curve data [38]. This latter work concentrated on the quite intricate interpretation of the experimental observations which revealed an astonishing dependence of the rocking-curve half-width on the so-called azimuthal angle which refers to the angle through which the specimen is rotated for a particular reflection around the normal to the reflecting glide planes. As said before in Section 2.2, it is emphasized that, in the case of ideally [001]-orientated crystals, any lattice plane misorientations can arise only, if deviations from ideally symmetric multiple slip occur. Here, we wish to discuss mainly the dependence of the rocking-curve half-width on the deformation. In reference [38], rocking-curve half-widths, obtained from {002} X-ray reflections, are reported for three states of deformation between resolved shear strains of 0.068 and 0.52 and between shear flow stresses of 26.2 and 75.6 MPa. These data were analyzed with the following results [22]:

- The maximal rocking-curve half-widths increase more weakly than linearly with the flow stress and can be represented quite well by a proportionality to the square root of the resolved shear strains, i.e.

$$\Delta\beta_{1/2} \propto \left(\sqrt{\gamma} - \sqrt{\gamma_o}\right), \text{ with } \gamma_o \approx 0.014. \qquad (21)$$

- According to Pantleon and Hansen [35] and Pantleon [36], the proportionality $\Delta\beta_{1/2} \propto \sqrt{\gamma}$ implies that the dislocation cell walls of the deformed [001]-orientated copper single crystals must be considered as incidental dislocation boundaries (IDBs) in the terminology of reference [37]. On the other hand, it is interesting to note that misorientations develop only after the resolved shear strain has exceeded a value of about 0.014. This implies that, up to that shear strain, multiple slip is ideally symmetric and that misorientations occur only later, probably as a result of statistical deviations leading to an instability of ideally symmetric multiple slip.

The above dependence of the misoríentations on the shear strains was first advocated by Argon and Haasen [39] as a consequence of an accumulation of random fluctuations in the fluxes of dislocations coming from either side of the cell wall. Frank Nabarro made a more specific calculation and derived, with some assumptions, the proportionality constant [40]. The more rigorous statistical derivation with an accurate determination of the proportionality constant was then performed by Pantleon [36].

4. The simultaneous contribution of GNDs to internal stresses and lattice plane misorientations – effects of relaxation of internal stresses

In the idealized cases considered so far, the GNDs either gave rise to deformation-induced long-range internal stresses (Section 2) or to deformation-induced lattice-plane misorientations (Section 3). However, in realistic dislocation distributions one and the same GND pattern can in general contribute simultaneously to both effects. If we consider as a ftrst example single slip in PSBs (figure 1), then it is clear that in this case no misorientations occur, because it is assumed implicitly that the PSB slab which is embedded in the surrounding matrix is so heavily constrained that to-and-fro bending due to the GND arrays is suppressed, as will be discussed in more detail elsewhere [22]. Once bending is allowed to occur to a certain extent, some misorientations will develop and, at the same time, the long-range internal stresses will relax partially. Thus, the GNDs will be the source of both the somewhat relaxed internal stresses and the misorientations that can develop as a consequence of relaxation. Since relaxations of this type must be considered as very likely, it appears realistic to conclude that, in general, one and the same GNDs contribute partially to giving rise to long-range internal stresses and partially to inducing lattice plane misorientations. However, without a more detailed model, there is no one-to-one relationship between these two contributions of GNDs. It follows from these dislocation-specific features that the “elastic

accommodation factor" Γ (that was introduced in a formal sense in Section 2.1), when applied to dislocation problems, loses some of the meaning that it had in Eshelby's original continuum mechanics treatment of the "inclusion problem" [41]. It is emphasized that, in the original composite model which was formulated as a Masing model [6,16], elastic accommodation was not taken into account. In later work, the Eshelby accommodation factor was introduced in a rather formal sense, like here, and it was emphasized that the experimental data suggest strongly that elastic accommodation is negligible ($\Gamma \approx 1$) in contrast to the result that one would obtain, if one modelled the dislocation walls as an Eshelby ellipsoid [7].

Considering multiple slip as another example and referring to figure 2, it is clear that any deviation from symmetric multiple slip will lead to misorientations in addition to the long-range internal stresses discussed previously. Finally, considering the very schematic illustration of the dislocation kink walls in figure 7, it would be unrealistic to assume that deformation (in particular at low temperatures) produces such idealized low-energy low-angle boundary patterns. Rather, in a more realistic picture, deviations must be expected which will then give rise to some long-range internal stresses in addition to the misorientations. Similar reasoning applies to the sheets/grids in work hardening stage II that were discussed briefly in Section 3.2. In all cases, the consequences with respect to the role of the GNDs acting simultaneously as sources of both internal stresses and of lattice plane misorientations will be similar as discussed above. Hence, an unequivocal identification and separation of the roles of the GNDs acting as either sources of long-range internal stresses and/or sources of lattice plane misorientations will not be straightforward without additional information in the form of more specific models or will have to be based on assumptions.

Nonetheless, the data on GND densities available so far (Sections 2.1.1, 2.2, 3.2, 3.4) indicate consistently that both the GND density responsible for the internal stresses and the density of those GNDs that give rise to misorientations increase with increasing deformation in a similar fashion and in such a manner that the ratio ρ_{GND}/ρ, referring to *all* GNDs, remains almost constant.

5. Concluding remarks

The preceding discussion which was based largely on an assessment of experimental X-ray diffraction data obtained on cyclically and unidirectionally deformed crystals, is regarded as a first step towards achieving a unified picture of the role of GNDs in the development of the

dislocation pattern during plastic deformation. In this picture, the GNDs are inseparably related to the evolution of both long-range internal stresses and/or lattice plane misorientations during plastic deformation. Both features are typical of macroscopically homogeneous but microscopically nonhomogeneous deformation. The following results of the (semi-)quantitativeanalysis of the deformation-induced long-range internal stresses and/or lattice plane misorientations in cyclically and tensile-deformed copper single crystals and the roles played by the GNDs in this context are considered noteworthy:

- The composite model takes full account of the deformation-induced long-range internal stresses but does not explain *per se* the evolution of lattice plane misorientations.
- With plausible modifications such as taking into account (partial) internal stress relaxation and deviations from ideally symmetric multiple slip, the composite model can provide information on deformation-induced misorientations.
- The stresses acting locally in the hard cell walls and in the soft cell interiors, respectively, and the magnitudes of the corresponding internal forward and back stresses, respectively, increase in good approximation linearly with the applied stress.
- From the analysis of the evolution of the lattice plane misorientations during deformation it could be concluded that the dislocation kink walls and the dislocation sheets/grids formed in single-slip deformation in work-hardening stage II are so-called geometrically necessary boundaries (GNBs), whereas the dislocation cell walls formed in multiple slip deformation are so-called incidental dislocation boundaries (IDBs).
- In general, it is concluded that one and the same GND pattern contributes to both the long-range internal stresses and the lattice plane misorientations.
- In all cases analysed, either with respect to the internal stresses or with respect to the misorientations, the density of the GNDs was found to be small, representing a fraction of the total dislocation density which amounts to only to a few percent and remains almost constant throughout deformation.

The examples discussed here represent typical selected and particularly simple situations characteristic of plastic deformation of copper single crystals. It is assumed that these results are also characteristic of other deformed fcc crystals. It can be envisaged that, in a next step, the same underlying principles can be applied in order to study more complex situations such as, for example, the role of GNDs in the microstructural evolution in individual grains of plastically deformed polycrystals [42]. Since, at present, X-ray diffraction techniques are probably the most appropriate tool to study these features of the dislocation pattern, there is

hope that, in such future experiments, today's possibilities of high-energy high-intensity synchrotron radiation, compare e.g. [42,43,44], will be utilized and allow to obtain more systematic results and of higher accuracy than in this study.

Acknowledgments

It is a pleasure to thank Professor Frank Nabarro for constructive criticism and for most inspiring discussions over many years. Sincere thanks go to Dr. Ellen Hieckmann for making available unpublished data. The present work rests on the valuable experience gained more than two decades ago at the Max-Planck-Institut für Metallforschung in Stuttgart under the guidance of the late Dr. Manfred Wilkens and Professor Alfred Seeger to whom I express my gratitude.

References

[1] F.R.N. Nabarro, Z.S. Basinski and D.L. Holt, Adv. Phys. **13** 193 (1964).
[2] A. Seeger, in *Work Hardening*, edited by J.P. Hirth and J. Weertman (Gordon and Breach, New York, 1968), p. 27.
[3] P.B. Hirsch, in *The Physics of Metals, 2. Defects*, edited by P.B. Hirsch (Cambridge University Press, 1975), p. 189.
[4] S.J. Basinski and Z.S. Basinski, in *Dislocations in Solids*, edited by F.R.N. Nabarro (North-Holland Publishing Co., 1979), Vol. 4, p. 261.
[5] H. Mughrabi, in *Constitutive Equations in Plasticity*, edited by A.S. Argon (MIT Press, Cambridge, Massachusetts and London, 1975), p. 199.
[6] H. Mughrabi, Acta Metall. **31** 1367(1983).
[7] H. Mughrabi and T. Ungár, in Dislocations in Solids, edited by F.R.N. Nabarro and M.S. Duesberry (Elsevier Science, B.V., 2002), Vol. 11, p. 343.
[8] M. Wilkens, Can. J. Phys. **45** 567(1967).
[9] M. Wilkens, in *Microstructural Charakterization of Materials by Non-Microscopical Techniques*, *Proceedings of 5th Risoe International Symposium on Metallurgy and Materials Science,* edited by N. Hessel Anderson et al. (Risoe National Laboratory, Roskilde, Denmark, 1984), p. 153.
[10] H. Mughrabi and B. Obst, Z. Metallkd. **96** 686(2005).
[11] A.H. Cottrell, *The Mechanical Properties of Matter* (John Wiley & Sons, Inc. New York, 1964), p. 277.
[12] M.F. Ashby, Phil. Mag. **21** 399(1970).
[13] F.R.N. Nabarro, private communication (2004/2005).
[14] Viewpoint Set No. 28: *"Geometrically Necessary Disocations and Size Dependent Plasticity"*, edited by A. Needleman and J. Gil Sevillano, Scripta Mater. **48** 109-183(2003).
[15] A. Needleman and J. Gil Sevillano, in ref. [14], p. 109.
[16] H. Mughrabi, in *Proceedings of 5th International Conference on the Strength of Metals and Alloys*, edited by P. Haasen, V. Gerold and G. Kostorz (Pergamon Press, 1980), Vol. 3, p. 1615.
[17] H. Mughrabi and F. Pschenitzka, in *Special Issue Dedicated to Professor David Embury,* Phil. Mag., in press.

[18] E. Hieckmann, private communication (2004/2005).
[19] H. Mughrabi, T. Ungár, W. Kienle and M. Wilkens, Phil. Mag. **53** 793(1986).
[20] T. Ungár, H. Mughrabi, M. Wilkens and A. Hilscher, Phil. Mag. A, **64** 495(1991).
[21] T. Ungár, H. Mughrabi, D. Rönnpagel and M. Wilkens, Acta Metall. **32** 333(1984).
[22] H. Mughrabi, presented at *International Conference on Micromechanics and Microstructure Evolution: Modeling, Simulation and Experiments*, Madrid, Sept. 2005, submitted to Proceedings, to appear in Special Issue of Acta Materialica.
[23] H. Mughrabi, Mater. Sci. Eng. A **317** 171(2001).
[24] H. Mughrabi, Mater. Sci. Eng. A **387** 209(2004).
[25] B. Obst, H. Auer and M. Wilkens, Mater. Sci. Eng. **3** 41(1968/69).
[26] J.C. Grosskreutz and H. Mughrabi, in *Constitutive Equations in Plasticity*, edited by A.S. Argon (MIT Press, Cambridge, Massachusetts and London, 1975), p. 251.
[27] M. Wilkens, K. Herz and H. Mughrabi, Z. Metallkd. **71** 376(1980).
[28] F. Ackermann and H. Mughrabi, unpublished work, 1976.
[29] H. Mughrabi, Mater. Sci. Eng. **33** 207 1978
[30] C. Buque, J. Bretschneider, A. Schwab and C. Holste, Mater. Sci. Eng. A **300** 254(2001)
[31] Y. Li, S.X. Li and G.Y. Li, Mater. Sci. Eng. A **372** 75(2004).
[32] P.B. Hirsch, in *Progress in Materials Science*, edited by B. Chalmers and R. King (Pergamon Press, 1956), Vol. 6, p. 283.
[33] R.W.K. Honeycombe, J. Inst. Metals **80** 49(1951-52).
[34] S. Mader and A. Seeger, Acta Metall. **8** 513(1960).
[35] W. Pantleon and N. Hansen, Mater. Sci. Eng. A **309-310** 246(2001).
[36] W. Pantleon, Solid State Phenomena **87** 73(2002).
[37] D. Kuhlmann-Wilsdorf and N. Hanse, Scripta Metall. Mater. **25** 1557(1991).
[38] M. Wilkens, T. Ungár and H. Mughrabi, Phys. Stat. Sol. (a) **104** 157(1987).
[39] A.S. Argon and P. Haasen, Acta Metall. Mater. **41** 3289(1993).
[40] F.R.N. Nabarro, Scripta Metall. Mater. **30** 1085 (1994)..
[41] J.D. Eshelby, Proc. Roy. Soc. London A **241** 376(1957).
[42] W. Pantleon, H.F. Poulsen, J. Almer and U. Lienert, Mater. Sci. Eng A **387** 339(2004).
[43] S.F. Nielsen, E.M. Lauridsen, D. Juul-Jensen, M;ater. Sci. Eng. A **319-321** 179(2001).
[44] R.I. Barabash, G.E. Ice, B.C. Larson and W. Yang, in Fundamental Research Series, *"From Proteins to Semiconductors: Beyond the Average Structure"*, (Kluwer/Academic/ Plenum Publishers, 2002), p. 49.

Figure Captions

Figure 1: Composite model of single slip in the PSB wall structure. a) Schematic illustration of dislocation distribution and glide processes. Note GNDs at the wall/channel interfaces. b) Compensation of shear strain mismatch bezween channels and walls by GNDs. c) redistribution of the locally acting stresses. From [6].

Figure 2: Composite model for symmetric multiple slip. a) Schematic illustration of showing two intersecting symmetrical slip systems with the accumulation of GNDs at the cell wall peripheries. b) Replacement of pairs of glide GNDs of Burgers vectors $\mathbf{b_1}$ and $\mathbf{b_2}$ by resultant Burgers vector b_{res} lying parallel to the walls. Schematic illustration of long-range internal stresses set up in the cell interiors and in the cell walls. From [6,16].

Figure 3: Local flow stresses τ_w-τ_o, τ_c-τ_o versus applied stress τ-τ_o in tensile-deformed Cu-1.4 at.%Mn single crystals. $\tau_o \approx 10$ MPa: solid solution friction stress. The faint line under 45° refers to the case of equality of local and applied stresses, i.e. absence of internal stresses. Data of Hilscher from [20].

Figure 4: Large-scale tilt misorientations around line direction of primary edge dislocations (Burgers vector $\mathbf{b_p}$) in the PSB wall structure.of copper single crystal deformed cyclically at a plastic shear strain amplitude of $\gamma_{pl} = 5\times10^{-3}$. a) X-ray Berg-Barrett topograph of primary (111) glide plane, showing orientation contrast. Note different scales in vertical and horizontal directions. b) Low-magnification TEM micrograph of section parallel to primary glide plane (111), showing long-range changes in background contrast. After [28].

Figure 5: Low-magnification TEM micrograph of $(1\bar{2}1)$-section of copper single crystal deformed cyclically at a plastic shear strain amplitude of $\gamma_{pl} = 1.45\times10^{-2}$. The changes in background contrast due to variations of local orientations should be noted. After [28].

Figure 6: Experimental evidence of dislocation kink walls in copper single crystals deformed into work hardening stage II. a) TEM micrograph of section parallel to (101) plane containing the primary Burgers vector $\mathbf{b_p}$, showing dipolar edge dislocation kink-wall cluster. From [5].

b) X-ray Berg-Barrett topograph of primary glide plane (111), showing orientation contrast around the axis $[1\bar{2}1]$. Courtesy of B. Obst [25].

Figure7: Schematic model of GND distribution in kink bands. *D*: kink wall spacing, *h*: vertical spacing between GNDs, β: average angle of misorientation. Primary Burgers vector $\mathbf{b_p}$ is horizontal. From [10].

Figure 8: Maximal halfwidths $\Delta\beta_{1/2}$ of X-ray rocking curves, obtained with different reflections with azimuthal positions for which the component of $[1\bar{2}1]$ axis perpendiculat to plane of incidence is maximal, plotted against shear flow stress τ. From [10].

Figures

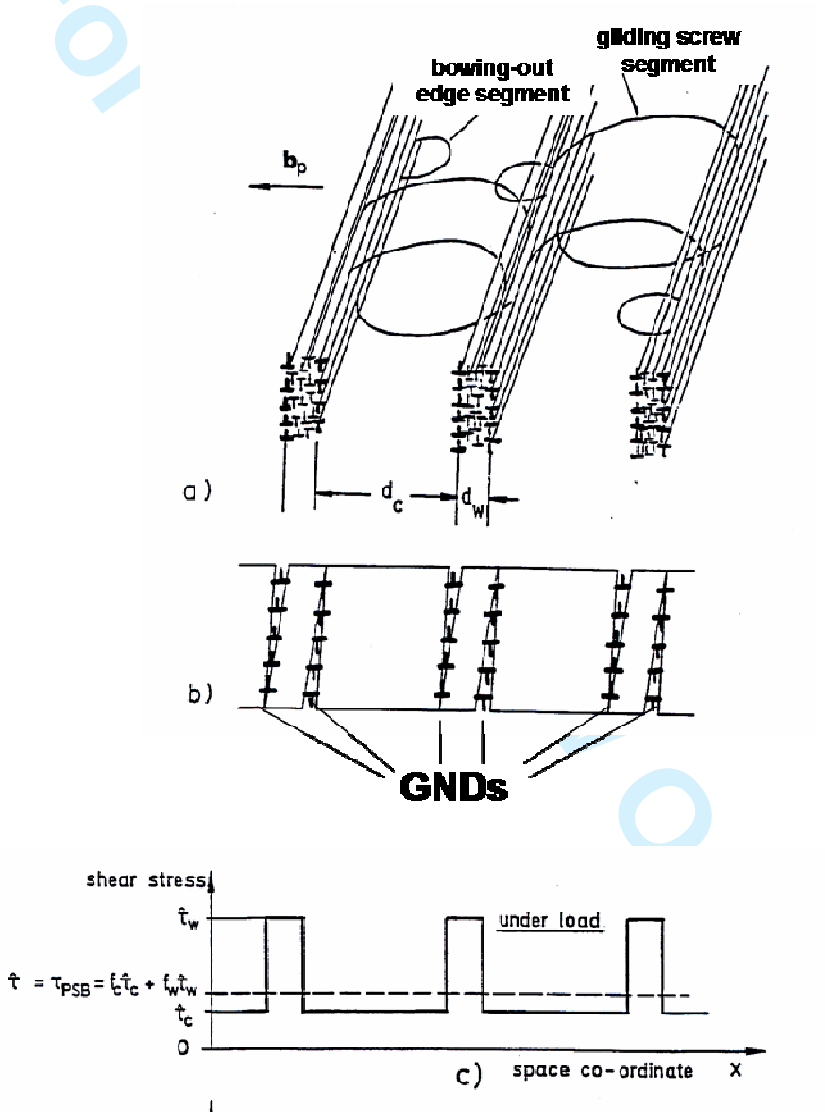

Figure 1

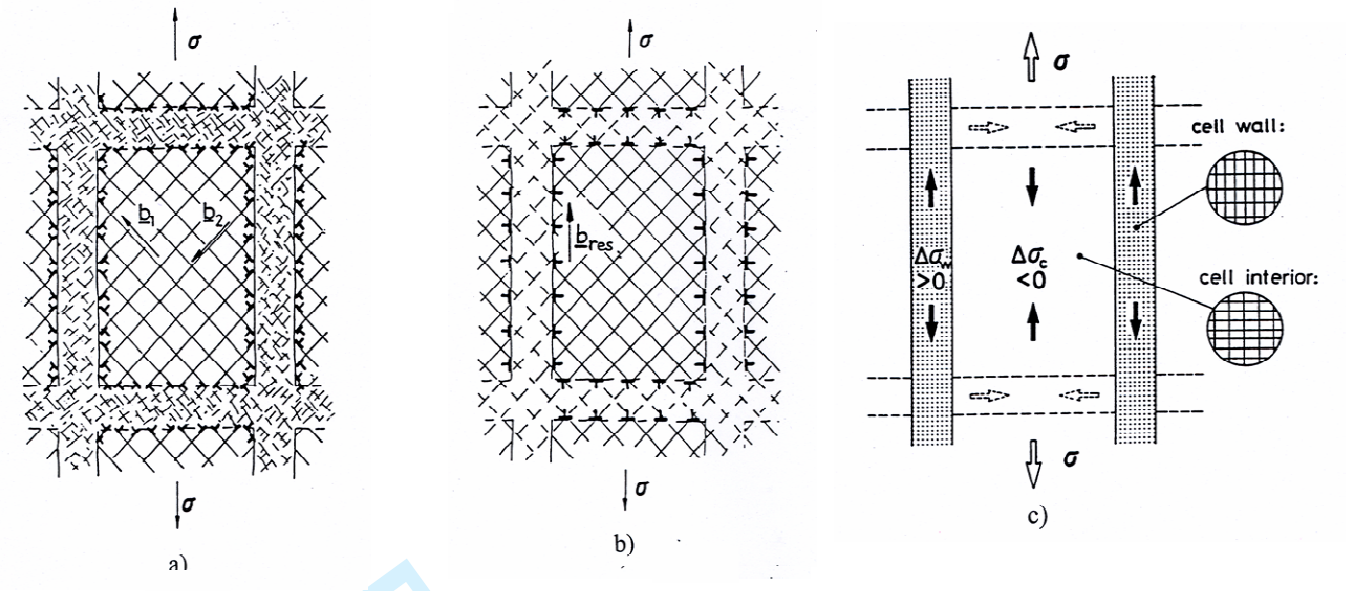

Figure 2

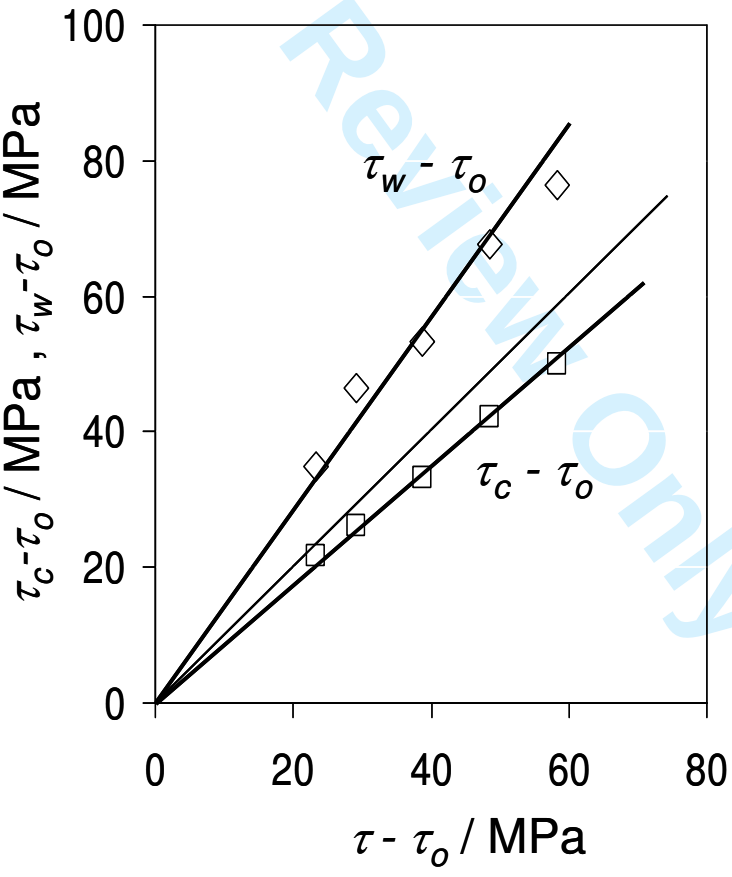

Figure 3

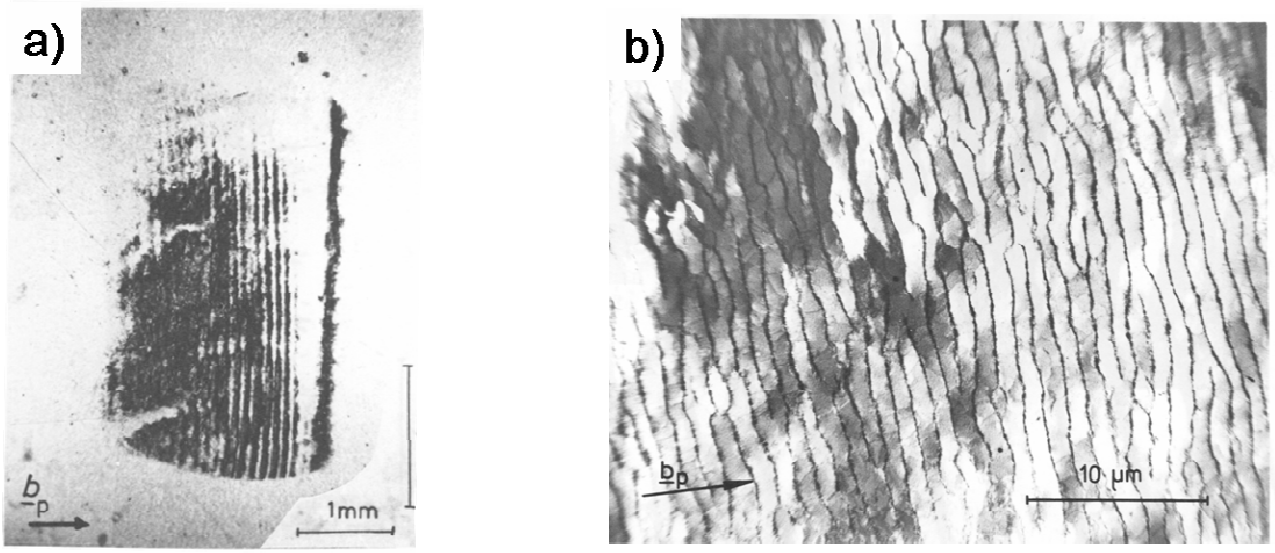

Figure 4

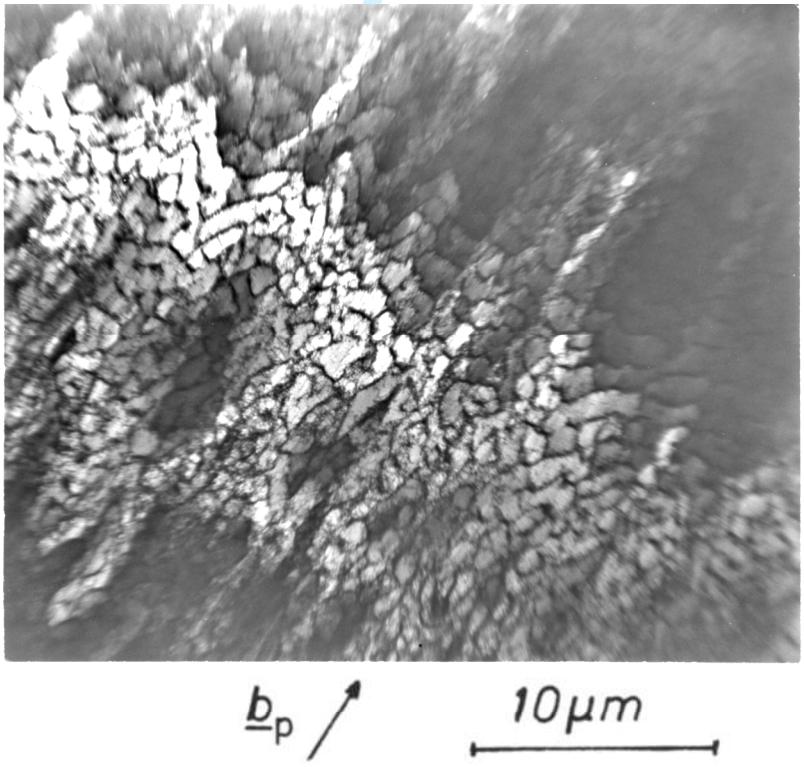

Figure 5

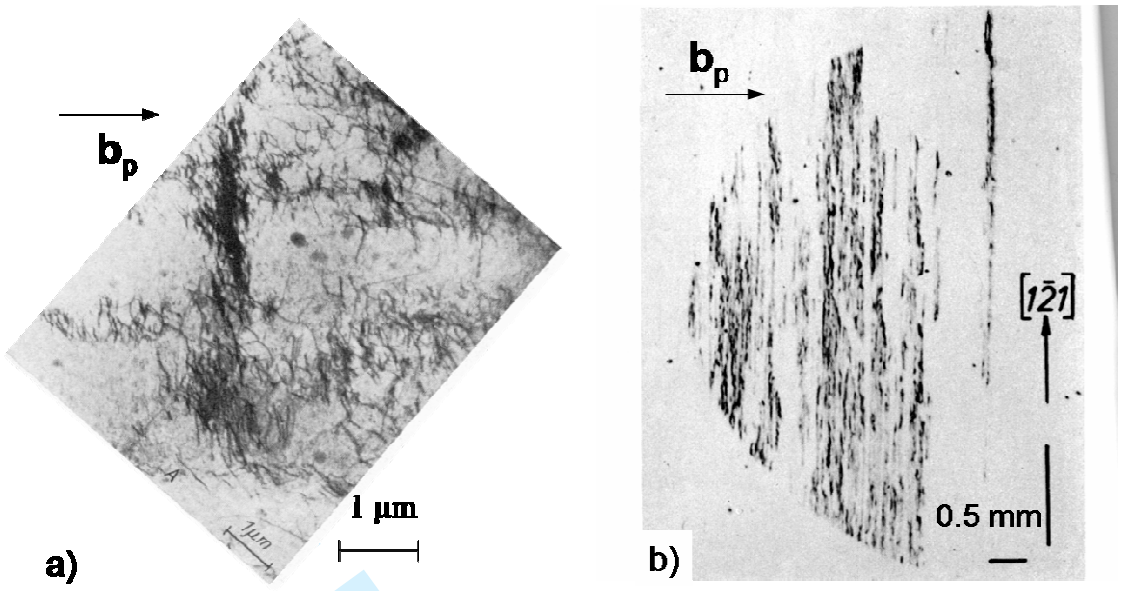

Figure 6

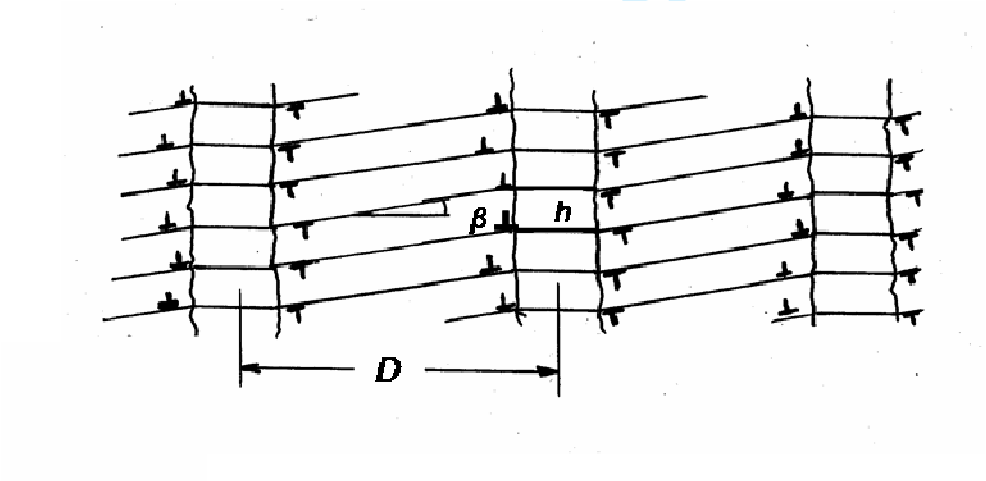

Figure 7

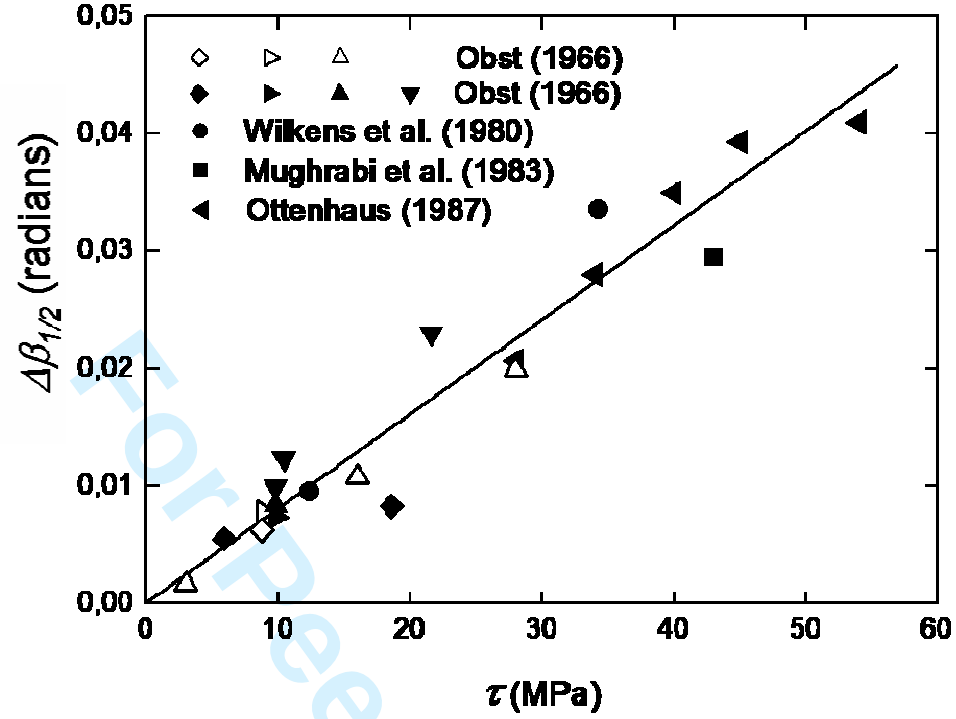

Figure 8